Supporting information

Flowerlike FePt/MnO_2/GOx-Based Cascade Nanoreactor with Sustainable O_2 Supplying for Synergistic Starvation-Chemodynamic Anticancer Therapy

Yunkai Kou,[a] Zhichao Dai,*[a] Ping Cui,[a] Zunfu Hu,[a] Lu Tian,[a] Feifei Zhang,[a] Haiqiang Duan,[a] Qiying Xia,*[a] Qingyun Liu,[b] Xiuwen Zheng*[a]

[a]Key Laboratory of Functional Nanomaterials & Technology in Universities of Shandong, School of Chemistry & Chemical Engineering, Linyi University, Linyi 276005, P. R. China

[b]College of Chemical and Environmental Engineering, Shandong University of Science and Technology, Qingdao 266590, P. R. China

*Corresponding authors.

Tel./Fax: +86-539-7258629

E-mail: zc_dai@126.com (Z. D.); xiaqiying@163.com (Q. X.); zhengxiuwen@lyu.edu.cn (X. Z.).

Physical measurements. Transimission election microscopy(TEM) images, high-resplution TEM (HRTEM) images and energy dispersive spectroscopy (EDS) spectra were determined on a JEOL-2100 transmission electron microscope. High-angle annular dark-field (HAADF)-scanning transmission electron microscopy (STEM) coupled with EDS elemental mapping was conducted on a JEOL ARM-200F field emission transmission electron microscope. Dynamic light scattering (DLS) and Zeta potential were detected by Nano-ZS (Malvern). The content of iron, platinum, and manganese was determined on a Thermo Fisher inductively coupled plasma (ICP) optical emission spectrometry (iCAP Qc). The UV-vis spectra and the fluorescent spectra were carried out on a NANO DROP 2000 spectrophotometer and an Edinburgh FS5 spectrophotometer, respectively.

Statistical Analysis. Statistical analysis was obtained by Student's t-test for three/four groups. The two-way ANOVA was used to evaluate the data of tumor growth using the Origin software. All results were expressed as the mean ± SD. A value of $p < 0.05$ was considered statistically significant.

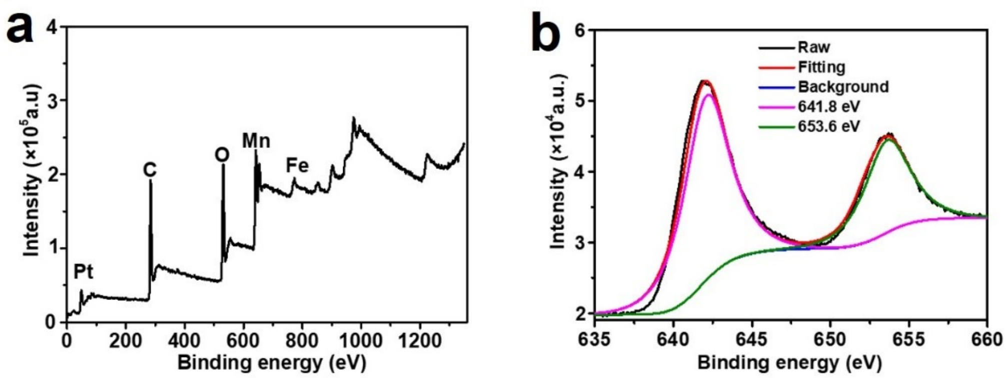

Fig. S1 XPS analysis of BGMFP. a) XPS spectra of BGMFP. b) XPS high-resolution scans of Mn2p peaks in BGMFP.

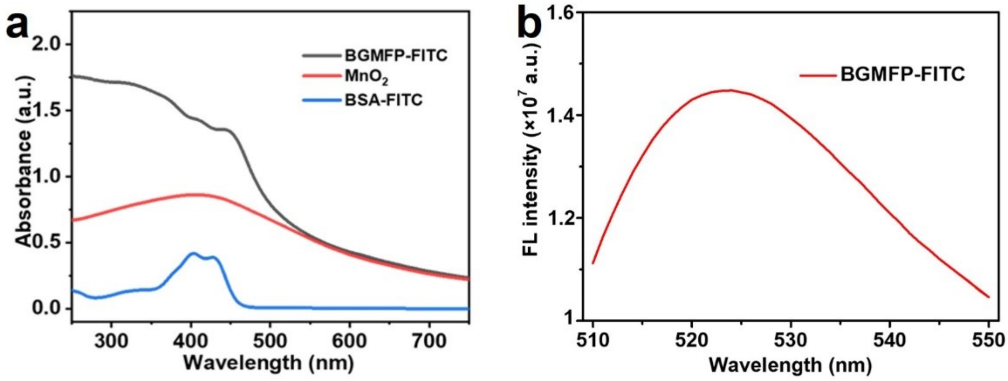

Fig. S2 The UV-vis absorption (a) and fluorescence (b) spectra of BGMFP-FITC.

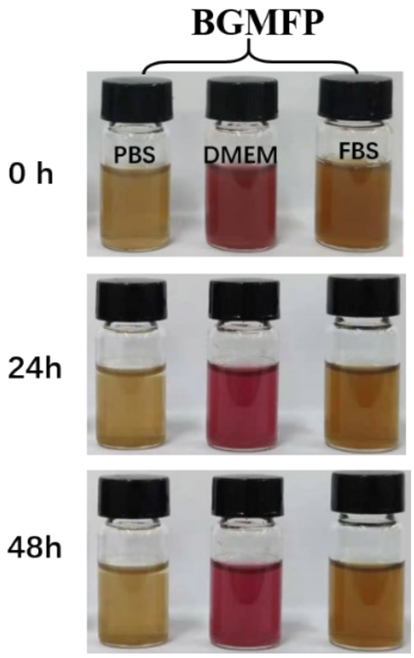

Fig. S3 The stability of BGMFP in PBS, DMEM and fetal bovine serum (FBS) after 48 h.

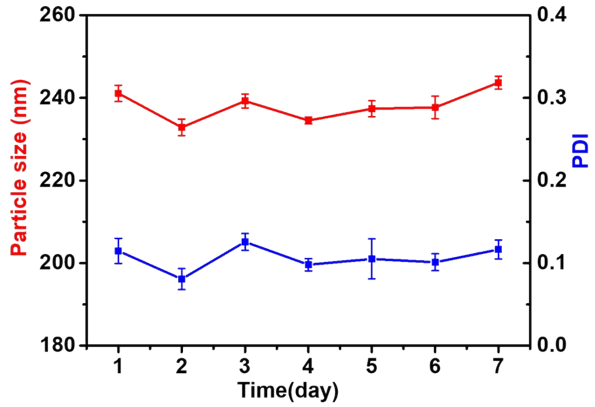

Fig. S4 The changes of hydrodynamic size and PDI of BGMFP size distribution and PDI changes of BGMFP within 7 days.

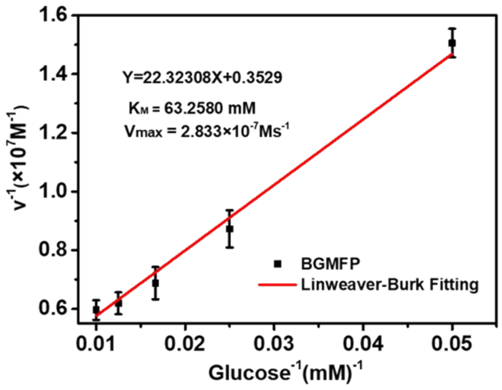

Fig. S5. Lineweaver-Burk plotting of BGMFP.

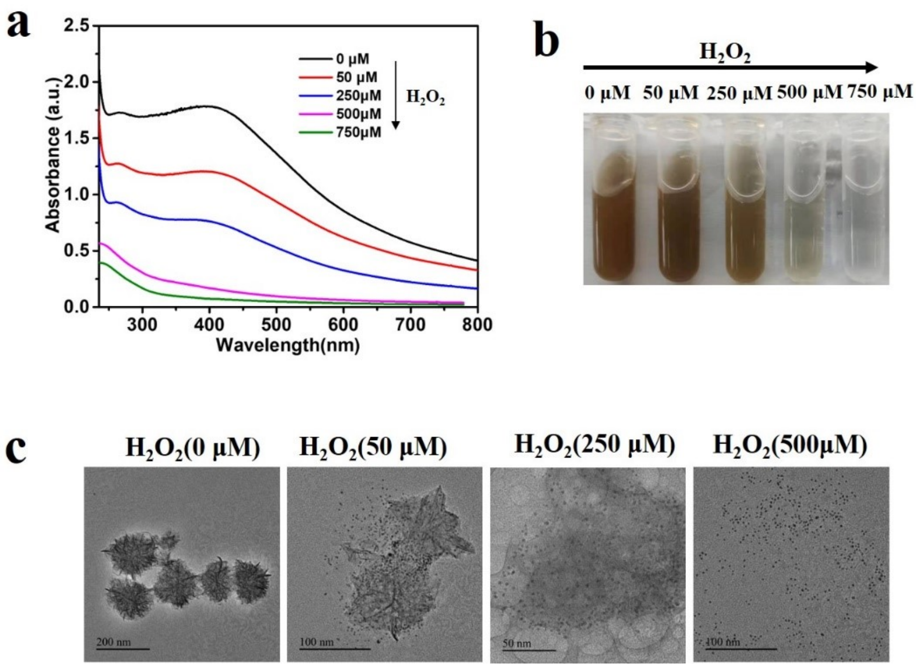

Fig. S6 The UV-Vis absorption spectra (a), digital photographs (b) and TEM images (c) of BGMFP(100 μg/mL) after treatment with H_2O_2 at different concentrations of pH 5.8.

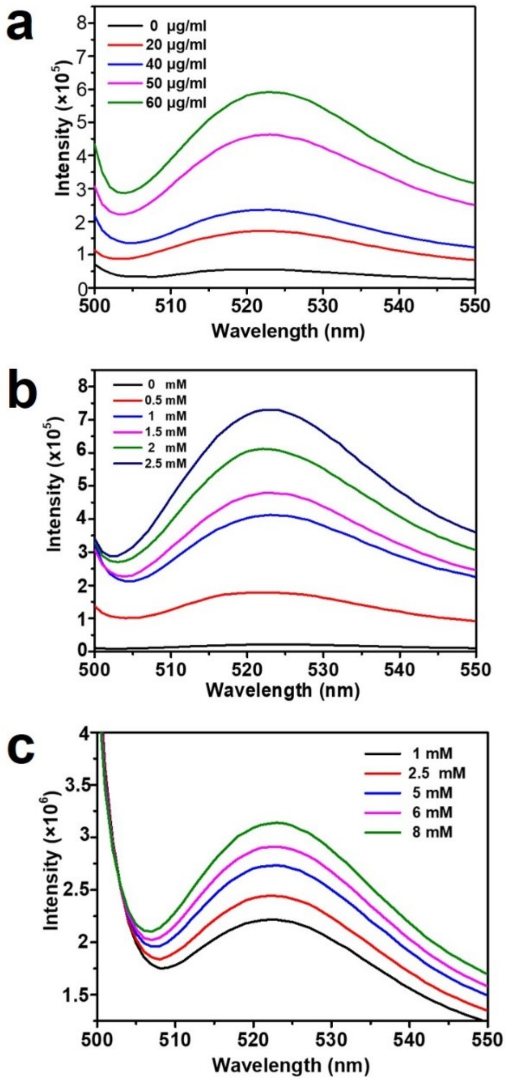

Fig. S7 The fluorescence spectra of DCFH with the increase of BGMFP (a), H_2O_2 (b) and glucose (c) content.

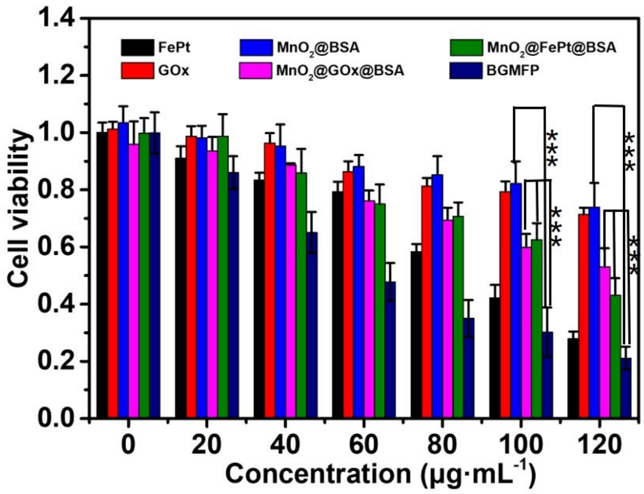

Fig. S8 The viability of 4T1 cells in different groups under hypoxia conditions. *p < 0.05, **p < 0.01, ***p < 0.005 (t-test).

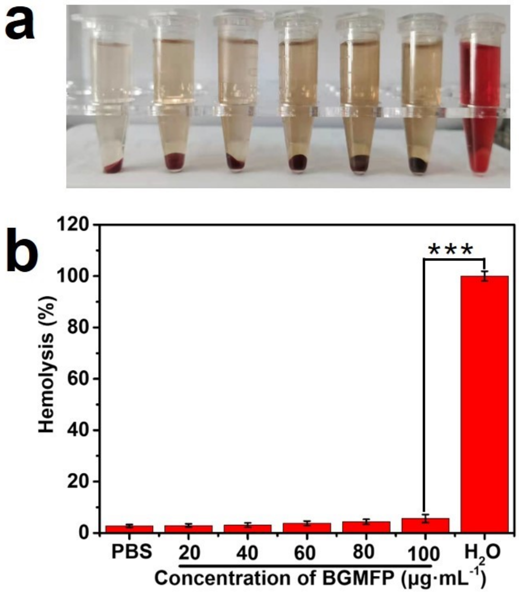

Fig. S9 (a) Photograph of RBC suspensions after treatment with various concentrations of BGMFP. The RBC suspensions treated with PBS and H_2O were set as negative control and positive control, respectively. (b) Corresponding hemolysis rates of the RBC samples in (a). (***$p < 0.005$).

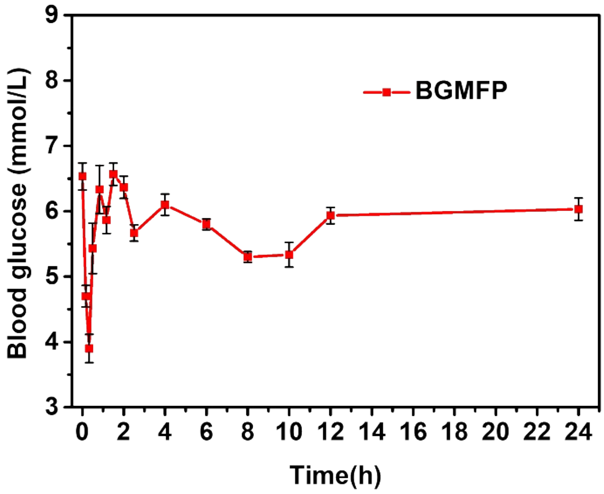

Fig. S10 The variations of blood glucose concentration in mice within 24 h after injection with BGMFP via tail vein.

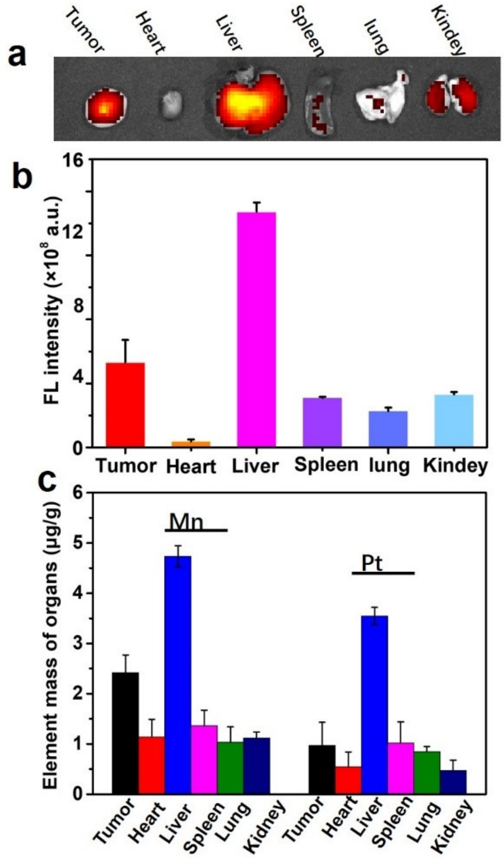

Fig. S11 (a) The fluorescence images of tumor and main organs derived from the mice at 108 h post injection. (b) The corresponding fluorescence intensity of (a). (c) The Pt/Mn level of tumor and main organs derived from the mice after 15 d treatment.

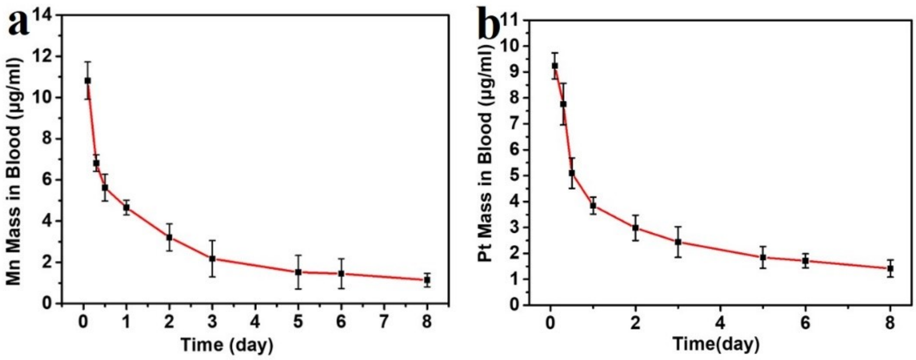

Fig. S12 The content of Mn (a) and Pt (b) in mice blood after the injection of BGMFP via tail vein.

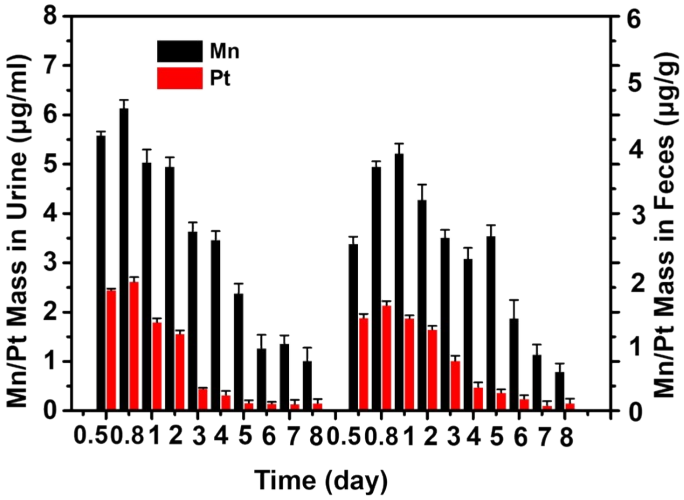

Fig. S13 Mn/Pt Content in feces and urine within 8 days.

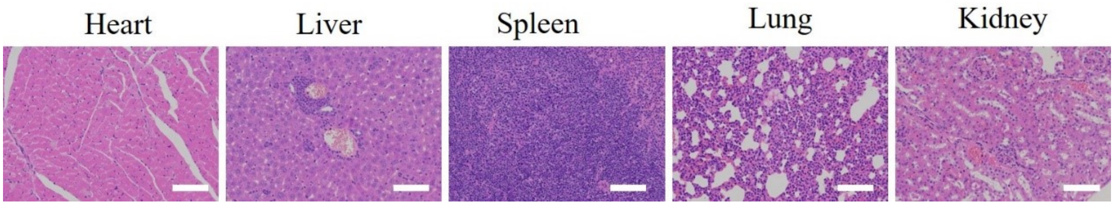

Fig. S14 H&E stained images of dissected major organs derived from the mice after treatment with BGMFP for 15 days (scale bars: 100 μm).